Submitted: *Science*

Date: 01/20/2009

Revised: 05/07/2009

Polarization Control of Electron Tunneling into Ferroelectric Surfaces

Peter Maksymovych*[1], Stephen Jesse[1], Pu Yu[2], Ramamoorthy Ramesh[2],

Arthur P. Baddorf[1], and Sergei V. Kalinin[1]

[1] Center for Nanophase Materials Science, Oak Ridge National Laboratory, Oak Ridge, TN, 37831

[2] Department of Materials Science and Engineering and Department of Physics, University of California, Berkeley, CA 94720

*corresponding author: maksymovychp@ornl.gov

Description

Switchable polarization of a thin film perovskite oxide controls the tunneling conductance of a nanoscale metal-ferroelectric junction by several orders of magnitude, enabling new approaches to high density non-volatile memory.

Abstract

We demonstrate a highly reproducible control of local electron transport through a ferroelectric oxide via its spontaneous polarization. Electrons are injected from the tip of an atomic force microscope into a thin film of lead-zirconate titanate, $(Pb(Zr_{0.2}Ti_{0.8})O_3$, in the regime of electron tunneling assisted by a high electric field (Fowler-Nordheim tunneling). The tunneling current exhibits a pronounced hysteresis with abrupt switching events that coincide, within experimental resolution, with the local switching of ferroelectric polarization. The large spontaneous polarization of the PZT film results in 100-fold amplification of the tunneling current upon ferroelectric switching. The magnitude of the effect is subject to electrostatic control via ferroelectric switching, suggesting possible applications in ultra-high density data storage and spintronics.

In quantum mechanics, a particle can tunnel through a potential barrier that exceeds the particle's energy. Tunneling underlies the operation of the resonant tunneling diode (*1*) and flash-memory (*2*), enables atomically resolved imaging in scanning tunneling microscopy (*3*) and holds promise for quantum computing based on SQUID magnetometers and quantum dots (*4, 5*). Replacing a conventional insulator in the tunnel junction with electronically correlated materials can

modify existing devices and yield new types of electronic functionality. In one of the earliest such concepts proposed by Esaki (*6*), dubbed a "polar switch," the tunneling barrier was composed of a ferroelectric oxide, which would have spontaneous, non-volatile polarization that could be switched in direction with an applied electric field. In a number of recent theoretical papers (*7*-*9*), including first-principles studies, the spontaneous polarization was predicted to modulate the height of the tunneling barrier, which would yield distinct nonvolatile conductance states that could subsequently be used to encode information. The density of the recorded information can potentially approach near-atomic limit, since the width of polarization domains in nanoscale ferroelectric oxides can be as small as several nanometers (*10, 11*).

It has proven difficult to find a material system that would simultaneously satisfy the dimensional constraints for tunneling and ferroelectricity. Ferroelectricity vanishes below a critical thickness, varying from 1 to 10 nanometers (*12, 13*), whereas direct tunneling is only feasible across a wide band-gap oxide thinner than ~2 nm. Although the polar distortion in perovskite oxides leading to ferroelectricity was recently reported even in three unit-cell (~1.2 nm) films (*11*), the presence of switchable polarization at this ultrathin limit has not yet been confirmed. Switching could be hindered by the formation of lamellar domain structures and a strong preference of the polarization to remain in the as-grown state (*14*). Gajek *et al*. (*15*) have recently demonstrated hysteresis of tunneling conductance through a 2-nm multiferroic film, albeit with a very small magnitude of <15%, as expected for the diminishing spontaneous polarization in such thin films (*12*). In addition to these fundamental physical constraints, the defect-rich nature of transition metal oxides often favors filamentary and defect-mediated conduction mechanisms over intrinsic tunneling (*16, 17*).

To demonstrate the polarization control of electron transport through a ferroelectric oxide, we used the tunneling barrier electronically defined at the junction between a sharp metal tip and the ferroelectric surface. We could thus avoid the necessity to reduce the oxide width, and work with relatively thick ferroelectric films (30 nm) with large spontaneous polarization. The electrons were injected into the oxide from the metal tip in the regime of Fowler-Nordheim (FN) tunneling (*18*) across an effectively triangular-shaped barrier. The FN-conductance was found to be strongly dependent on the polarization direction, which resulted in abrupt enhancement of current (up to 500-fold) at ferroelectric switching events.

We have studied the local transport properties of the (100)-oriented 30-nm ferroelectric film of tetragonal $Pb(Zr_{0.2}Ti_{0.8})O_3$ (PZT) using atomic force microscopy (AFM) in ultrahigh vacuum (UHV). The surface of the film was flat and had well-defined unit-cell steps (Fig. 1A). The preferred direction of spontaneous polarization is toward the bottom metallic $La_{0.7}Sr_{0.3}MnO_3$ (LSMO) electrode. The polarization could be readily switched in UHV, Fig. 1B, by biasing the AFM tip relative to the bottom electrode. The switching bias, determined from the piezoresponse hysteresis loops (*19*), varied across the surface because of the inherent disorder in the film with the averages of 1.3±0.6 V and -3.7±0.8 V for the positive and negative nucleation bias, respectively (Fig. 1C). The hysteresis loops also revealed a significant built-in potential across the film (~ 1.2 V).

Local current-voltage (I-V) characteristics (Fig. 1D) were highly rectifying with no current above the noise-floor (~ 40 pA) observed at positive tip bias. The shape of the I-V curve, however, depended strongly on the probed range of the tip bias. The onset of current was smooth, and the I-V curve exhibited little or no hysteresis between forward (increasing negative tip bias) and backward bias ramps if the positive bias was limited to < 0 V. In contrast, increasing the upper limit to >2 V yielded an abrupt current jump in the forward direction, followed by a continuous region and a

smooth reverse curve, Fig. 1E. The tip bias at the current discontinuity varied across the surface with an average value of -3.3±1.1 V. Because this voltage variation is well within the range of ferroelectric switching, (Fig. 1C), the observed current hysteresis may be related to the ferroelectric polarization of the surface. However, a rigorous correlation can be established only in a simultaneous measurement of the ferroelectric and conducting properties, because transition metal oxides can exhibit defect-mediated resistive switching (*16, 20, 21*) and charge injection from the AFM tip was previously shown to induce local conducting states in lead-zirconate films (*22*).

To acquire the local piezoresponse hysteresis loops (Fig. 1B), we applied an AC-bias to the AFM tip after subsequent DC-poling cycles (*19*). A typical AC-bias amplitude of > 0.5 V tended to smooth the observed ferroelectric switching event, and also interfered with the conductance measurements. Thus, we acquired local strain loops via a static displacement of the AFM tip during the DC-bias ramp (*23*). As seen in Fig. 2A, the strain loop in a symmetric bias window (+5 V to -5V) had a clear butterfly shape. The surface locally expanded (contracted) upon increasing bias until a ferroelectric switching event changed the deformation direction to compression (expansion). The statistical distributions of the switching bias from the strain and AC-piezoresponse measurements were similar, Fig. 3A, although the former yielded slightly smaller average values. This difference was likely caused by a relaxation effect, in that the occurrence of a stable reverse-polarity domain was detected at zero tip bias in the AC-technique and a non-zero value in the strain-loop measurements.

The discontinuities in the strain loop and the simultaneously acquired current hysteresis coincide at negative tip bias (Fig. 2A). This behavior was reproduced in all of ~ 600 hysteretic I-V curves acquired in different places on the PZT surface, a subset of which is shown in Fig. 2B. In about 10% of the hysteretic I-V curves, several discontinuities were observed that also displayed a

similar pattern of piezoelectric displacements (Fig. 2C). This response may be indicative of defect-mediated pinning of the reversed-polarization domain growth. At the same time, smooth I-V curves correlated only with continuous strain loops, where no ferroelectric switching occurs (Fig. 2D). Finally, the transition between smooth (Fig. 2D) and hysteretic I-V characteristics (Fig. 2A) occurs at the minimal positive bias required to open the butterfly-shaped strain loop (Fig. S1). These measurements rigorously establish the correlation between switching of ferroelectric polarization and electronic conductance. To rule out a possible involvement of residual adsorbates in the observed effects, we carried out a control experiment on a similarly grown 50 nm PZT/LSMO film, finding that annealing the film in 20 mTorr oxygen atmosphere at T = 600 K for 20 minutes had no observable effect on the polarization-dependent electron transport through the film (Fig. S2). We would like to add that the reproducibility of I-V curves across the surface distinguishes our results from those of filamentary conduction, because the spatial distribution of conducting filaments was shown to be very non-uniform (*17*). Also, highly rectifying I-V characteristics (Fig. 2A,C) are distinct from a previous study of a macroscopic ferroelectric capacitor, where the I-V curves became Ohmic after polarization switching (*24*).

Smooth I-V curves can be linearized in the coordinates $log(I/V^2) = f(V^{-1})$, which is a signature of Fowler-Nordheim tunneling through a triangular potential barrier. The FN-tunneling current (*18*),

$$I = A_{eff} \frac{e^3 m_{Pt}}{8\pi h m_{PZT} \phi_B} E^2 \exp\left(-\frac{8\pi\sqrt{2m_{PZT}}}{3he} \frac{\phi_B^{3/2}}{E}\right), \quad (1)$$

is a function of the barrier height ϕ_B, electric field, E, effective tunneling area, A_{eff}, and the effective electron mass in the tip (m_{Pt}, assumed ~ m_e) and PZT (m_{PZT}, assumed here ~$3m_e$). The observed current hysteresis implies that the FN-tunneling conductance is drastically reduced when the

polarization vector is anti-parallel to the applied electric field. Polarization switching is accompanied by changes in the local strain and electrostatics in the material, both of which can be the source of hysteresis.

We can rule out the nanomechanical origins, such as the local expansion of the material and the change of the tip-surface contact area A_{eff}. Indeed, this piezoelectric effect would increase the width of the tunneling barrier upon switching (*7*), leading to a drop in the tunneling conductance, opposite to the observed trend (Fig. 2A-C). The changes in the tip-surface contact area were ascertained to be insignificant by measuring the bias-dependence of the contact resonance of the cantilever (Fig. 3B). The frequency varied by only ~300 Hz across the whole bias range, corresponding to at most a two-fold change in the contact area (*25*).The current, however, increased by several orders of magnitude upon switching. Furthermore, the resonance frequency decreased at negative tip bias indicating that the contact area slightly decreases too. The FN-current hysteresis must therefore arise from electrostatic effects, originating from the screening of the bound polarization charge on ferroelectric surfaces (*7, 9*).

The barrier height in Eq. 1 corresponds to the height of the Schottky barrier at the metal-ferroelectric interface. The interfacial band alignment is influenced by the presence of bound dipoles (*26*). These dipoles may originate from dangling bonds or polar terminations in conventional semiconductors, whereas in ferroelectrics there is an additional strong component caused by the bound polarization charge. In the simplest one dimensional model, the metal and ferroelectric are separated by an ultrathin insulating layer that could arise from a non-epitaxial contact (between the tip and the surface in our case), the reacted surface layer, or the formation of an intrinsic dielectric dead-layer (*27*). The potential drop across the insulating layer rigidly shifts the electronic bands of the ferroelectric relative to the Fermi level of the tip (Fig. 3C). The change of the barrier height can

be estimated as $\Delta\phi_B = \frac{e\delta_I}{\varepsilon_I}\sigma_S$ (*26*), where δ_I is the width of the dielectric gap, ε_I its dielectric constant and σ_S is the surface charge density. The magnitude of σ_S is determined by the competition between internal and external screening of the polarization charge, as well as a possible suppression of the polarization charge in the vicinity of the interface (*27*). $\Delta\phi_B$ is ~0.7 eV for an estimated δ_I = 0.06 nm, $\varepsilon_I = \varepsilon_0$ and σ_S = 0.1 C/m^2. This difference is large enough to fully suppress FN electron tunneling into an oppositely polarized film, as observed experimentally.

Because the accumulation of positive surface charge on an upward polarized surface will shift the ferroelectric bands down in energy (Fig. 3C), the Schottky barrier for electron tunneling into the conduction band of the ferroelectric (n-type band alignment) will decrease in height. The n-type band alignment in the tip-surface junction is consistent with the observation of current at negative tip polarity. Therefore the external screening model predicts the right sign of the effect irrespectively of the detailed mechanisms. Our estimate also agrees with recent ab-initio calculations of an epitaxial $SrRuO_3/BaTiO_3/SrRuO_3$ capacitor, where the barrier height decreases by ~0.4 eV for upward polarization due to combined effects of electrostatics and local chemical bonding (*9*).

Fitting of Eq. 1 to the experimental I-V curves with the assumption of a 300 nm^2 contact area (20 nm tip diameter) reveals that the electric field has to exceed 5 MV/cm to allow tunneling across a realistic potential barrier of 0.8-1.0 eV between Pt and PZT (*28*). This value is at least five times higher than what would be achieved if the potential drop were uniform across the PZT film. The required non-uniformity can be produced by the sharpness of the metal tip producing a localized electric field in the vicinity of the surface, or by a relatively large total density of deep and shallow levels in the band-gap of the ferroelectric that yield narrow Schottky barriers via effective screening.

To assess the strength of a localized field, we have modeled the tip-surface junction as a disk in contact with a dielectric surface (*29*). Although the model fits the data very well (Fig. 3D), sufficiently localized fields in a dielectric substrate (or a fully depleted film) are produced if the tip-diameter is less than 5 nm (*25*), while the effective tunneling area is ~ 4 nm^2. These values are less than the expected tip diameter of >20 nm in contact-mode AFM. Thus, the localized field enhancement can take place if there is a sharp asperity on the tip surface that dominates the tunneling transport. Notably, although the potential drop across the film is non-uniform, it is almost identically linear several nanometers under the tip (Fig. S4), creating a narrow triangular potential barrier where the FN-tunneling equation applies.

The second possibility of thin Schottky barriers was previously invoked to rationalize the occurrence of Fowler-Nordheim tunneling in capacitor experiments with macroscopic electrodes (*30, 31*). Several works (*30, 32*) have reported a relatively high total density of rechargeable levels in $Pb(Zr_{0.2}Ti_{0.8})O_3$ films, up to 10^{20} cm^{-3}. The ferroelectric film can then be treated as a doped semiconductor, where the polarization charge is screened by charged and ionized defects (*33*). The depletion width and the corresponding maximum electric field (E_m) at the interface become polarization dependent. E_m can exceed 4 MV/cm already at a tip-bias of 2 V (*25*). Substituting the bias dependent E_m into the Eq. (1) also yields a good fit to the measured I-V curves (Fig. 3D), with an average barrier height of 1.1±0.1 eV, a realistic tunneling area of 300±6 nm^2 (tip diameter ~ 20 nm) and a spontaneous polarization of 0.4±0.1 C/cm^2. The depletion width in this model is polarization dependent, which will introduce strong current hysteresis in addition to that from the change of the barrier height.

Although we cannot determine which of the above models is dominant, we have observed similar local transport through 50 nm PZT films (Fig. S2) and 5 nm $BiFeO_3$ films (Fig. S3). The

barrier narrowing thus appears to be an intrinsic property of high-field transport in perovskite ferroelectrics, in agreement with a number of capacitor measurements (*30*). The polarization-dependence of the Schottky barrier height will have an equally pronounced effect on local conductance independently of the model, and it will also produce strong conductance hysteresis in the Schottky emission (*34*), another interface-limited conduction mechanism that exhibits exponential dependence on the barrier height.

The pronounced coupling between ferroelectricity and FN tunneling results in high-to-low conductance ratios up to 500:1 in the region of the current hysteresis, Fig. 4A. The conductance ratio grows exponentially with decreasing ferroelectric switching voltage, because the downward-polarized surface shows no conductance up to the switching voltage (Fig. 1C,D). The hysteresis observed in our measurements was already sufficient to demonstrate a prototype resistive memory action. Fig. 4B shows a series of consecutive write (+/- 5V) and read (- 2V) bias pulses, where the read voltage was chosen to yield measurable current on the upward-polarized surface. The memory effect is manifested in the ability to read-out the high (30-50 pA) and low (noise-limited to ~1 pA) conductance states, and to do so non-destructively (Fig. 4B) because the read bias was at least 1 V below the onset of ferroelectric switching. Theoretically, FN-conductance ratio can exceed five orders of magnitude, depending on the polarization-induced change of the barrier height, tip bias, size and material properties (Fig. S6). The hysteresis window can be optimized through the built-in field across the ferroelectric film, by varying its dimensions, doping and the choice of the bottom electrode and tip materials. This is exemplified in Fig. 4C,D for 50 nm PZT films grown on $SrRuO_3$ (SRO) and $La_{0.7}Sr_{0.3}MnO_3$ electrodes. The I-V curve on the PZT/SRO film revealed negligible hysteresis, because ferroelectric switching occurred in the bias-range where the film was insulating, Fig. 4C. Substituting SRO with LSMO produced strong built-in field, overlapping the bias range of

conductance and polarization switching events and creating a very pronounced conductance hysteresis, Fig. 4D.

The large magnitude of the conductance hysteresis, its tunability via ferroelectric switching and the ability to implement non-destructive resistive (rather than capacitive) read-out of polarization direction indicate the promise of ferroelectric Fowler-Nordheim tunneling in the development of ultra-high density information storage. According to a recent theoretical study, the minimum recordable domain size decreases with thickness, but passes through a minimum, increasing again for the thinnest films (*35*). A relatively weak thickness dependence of FN-tunneling will thus be critical in achieving the highest density of resistively readable information on a ferroelectric surface. The compatibility of FN tunneling with multiferroic oxides (such as $BiFeO_3$) also poses a possibility of implementing multiferroic control of this transport regime for spintronic applications. Finally, polarization-dependent transport can be used to study the ferroelectric property itself, in an attempt to reveal the switching mechanisms in nanoscale systems and explore the role of defects.

References

1. R. Tsu, L. Esaki, *Appl. Phys. Lett.* **22**, 562 (1973).
2. R. Bez, E. Camerlenghi, A. Modelli, A. Visconti, *Proceedings of the IEEE* **91**, 489 (2003).
3. G. Binnig, H. Rohrer, *IBM J. Res. Develop.* **30**, 4 (1986).
4. J. Majer *et al.*, *Nature* **449**, 443 (2007).
5. J. M. Elzerman *et al.*, *Nature* **430**, 431 (2004).
6. L. Esaki, R. B. Laibowitz, P. J. Stiles, *IBM Tech. Discl. Bull.* **13**, 2161 (1971).
7. H. Kohlstedt, N. A. Pertsev, J. R. Contreras, R. Waser, *Phys. Rev. B* **72**, 125341 (2005).
8. E. Y. Tsymbal, H. Kohlstedt, *Science* **313**, 181 (2006).
9. J. P. Velev *et al.*, *Nano Lett.* **9**, 427 (2009).
10. P. Aguado-Puente, J. Junquera, *Phys. Rev. Lett.* **100**, 177601 (2008).
11. D. D. Fong *et al.*, *Science* **304**, 1650 (2004).
12. J. Junquera, P. Ghosez, *Nature* **422**, 506 (2003).

13. C. H. Ahn, K. M. Rabe, J.-M. Triscone, *Science* **303**, 488 (2004).
14. V. Nagarajan *et al.*, *J. Appl. Phys.* **100**, 051609 (2006).
15. M. Gajek *et al.*, *Nat. Mat.* **6**, 296 (2007).
16. H. Kohlstedt *et al.*, *Appl. Phys. Lett.* **92**, 062907 (2008).
17. K. Szot, W. Speier, G. Bihlmayer, R. Waser, *Nat. Mat.* **5**, 312 (2006).
18. R. H. Fowler, L. W. Nordheim, *Proc. Roy. Soc. A* **119**, 173 (1928).
19. S. Jesse *et al.*, *Nat. Mat.* **7**, 209 (2008).
20. R. Waser, M. Aono, *Nat. Mat.* **6**, 833 (2007).
21. Y. Watanabe, *Ferroelectrics* **349**, 190 (2007).
22. C. Yoshida, A. Yoshida, H. Tamura, *Appl. Phys. Lett.* **75**, 1449 (1999).
23. S. Wicks, V. Anbusathiah, V. Nagarajan, *Nanotechnology* **18**, 465502 (2007).
24. P. W. M. Blom, R. M. Wolf, J. F. M. Cillessen, M. P. C. M. Krijn, *Phys. Rev. Lett.* **73**, 2107 (1994).
25. *Supporting material available on Science Online.*
26. R. T. Tung, *Phys. Rev. B* **64**, 205310 (2001).
27. A. K. Taganstev, G. Gerra, *J. Appl. Phys.* **100**, 051607 (2006).
28. I. Stolichnov, A. Tagantsev, N. Setter, J. S. Cross, M. Tsukada, *Appl. Phys. Lett.* **75**, 1790 (1999).
29. A. N. Morozovska, S. V. Kalinin, E. A. Eliseev, S. V. Svechnikov, *Ferroelectrics* **354**, 198 (2007).
30. J. F. Scott, *Ferroelectric Memories* (Springer, 2000).
31. I. Stolichnov, A. K. Taganstev, E. L. Colla, N. Setter, *Appl. Phys. Lett.* **73**, 1361 (1998).
32. L. Pintilie *et al.*, *J. Appl. Phys.* **98**, 124104 (2005).
33. L. Pintilie, M. Alexe, *J. App. Phys.* **98**, 124103 (2005).
34. S. M. Sze, *Semiconductor Devices: Physics and Technology, 2nd Ed.* (Wiley, 2001).
35. A. N. Morozovska, E. A. Eliseev, *Phys. B - Cond. Mat.* **373**, 54 (2006).
36. S. Jesse, A. P. Baddorf, S. V. Kalinin, *Nanotechnology* **17**, 1615 (2006).
37. Experiments were done at the Center for Nanophase Materials Sciences, Office of Basic Energy Sciences, U.S. Department of Energy. PM: Research performed as a Eugene P. Wigner Fellow and staff member at the Oak Ridge National Laboratory. The work at Berkeley is partially supported by the SRC-NRI-WINS program as well as by the Director, Office of Science, Office of Basic Energy Sciences, Materials Sciences Division of the U. S. Department of Energy under contract No. DE-AC02-05CH1123.

Figure captions

Figure 1. (A) Top-to-bottom: the surface topography of the PZT film imaged in the contact-mode; simultaneously acquired piezoresponse amplitude, revealing domains of upward (•) and downward (×) polarization (locally recorded by scanning a biased AFM tip) separated by a domain wall (black line); topographic profile along the red dashed line. (B) Fourty piezoresponse hysteresis loops taken at random locations on the surface of the PZT sample. Schematics show domain structures forming under the tip on the positive and negative branches of the hysteresis curves. (C) Distribution of the positive (red) and negative (blue) switching biases, measured at 3% of the total piezoresponse in the hysteresis loop. (D, E) I-V curves from three different locations on the surface acquired using a triangular ramp of tip bias from 0 V to -5 V (D) and from 5V to -5V in (E). The blue (red) curves are acquired during the forward (reverse) branch of the bias ramp from positive (negative) to negative (positive) values.

Figure 2. Simultaneous measurements of local conductance and piezoresponse on the surface of a 30 nm PZT film. The bias ranged from 5 V to –5 V for I-V curves in A, B and C, and from 0 V to –5 V for that in D. (B) Correlation between current and strain curves based on 126 measurements acquired on a 6400 nm^2 grid with a lateral resolution of 20 nm. Each horizontal line in the images corresponds to one forward I-V (left) and its matching strain (right) curve. Both I-V and strain curves in the data set were sorted according to the negative tip bias at current discontinuity. The discontinuities lie along the boundary of the blue and yellow regions. The boundaries are identical in the current and strain measurements, revealing the coincidence of the respective switching events. Streaks in the images correspond to the I-V/strain curves with double jumps as in (C).

Figure 3. (A) Distribution of the switching bias was determined from strain loops (blue) and AC-piezoresponse loops (red). (B) The measurement of the first contact resonance of the cantilever as a function of DC-bias. The amplitude of the oscillation varies due to non-local electrostatic effects (*36*). (C) Schematic polarization domain structure and interfacial band alignment for the low and high conducting states of the PZT film. Only the conduction band profile of the ferroelectric is shown. The dashed line corresponds to a uniform potential in the film, while the solid line is the schematic non-uniform distribution in the disk and thin Schottky barrier models. (D) Fitting of a smooth I-V curves (blue) to the modified Fowler-Nordheim equation in the framework of the disk-potential and thin Schottky barrier models (blue curve – data, red curve – fit, *a* - disk radius).

Figure 4. (A) High-to-low ratio of conductance as a function of the tip bias corresponding to ferroelectric switching from the analysis of 400 hysteretic I-V curves. (B) Prototypical memory action based on the ferroelectric control of Fowler-Nordheim tunneling. The blue curve is a pulse sequence which records (w) and reads-out (r) the high (logical 1) and low (logical 0) conductance states. The red curve is a current read-out. (C,D) Local I-V (top) and strain (bottom) curves on 50 nm PZT films with $SrRuO_3$ (C) and $La_{0.7}Sr_{0.3}MnO_3$ (D) bottom electrodes.

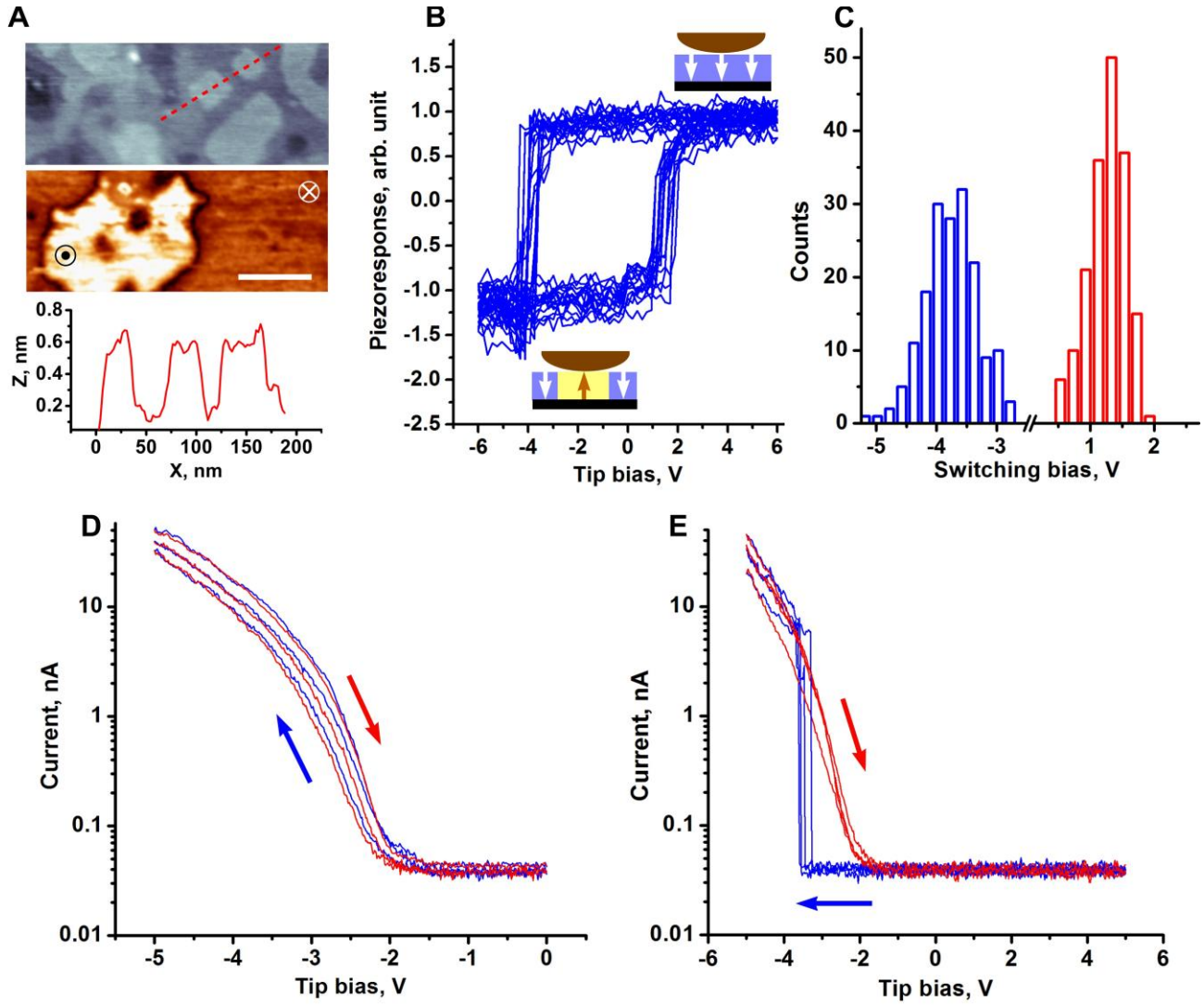
A
Z, nm
X, nm
B
Piezoresponse, arb. unit
Tip bias, V
C
Counts
Switching bias, V
D
Current, nA
Tip bias, V
E
Current, nA
Tip bias, V

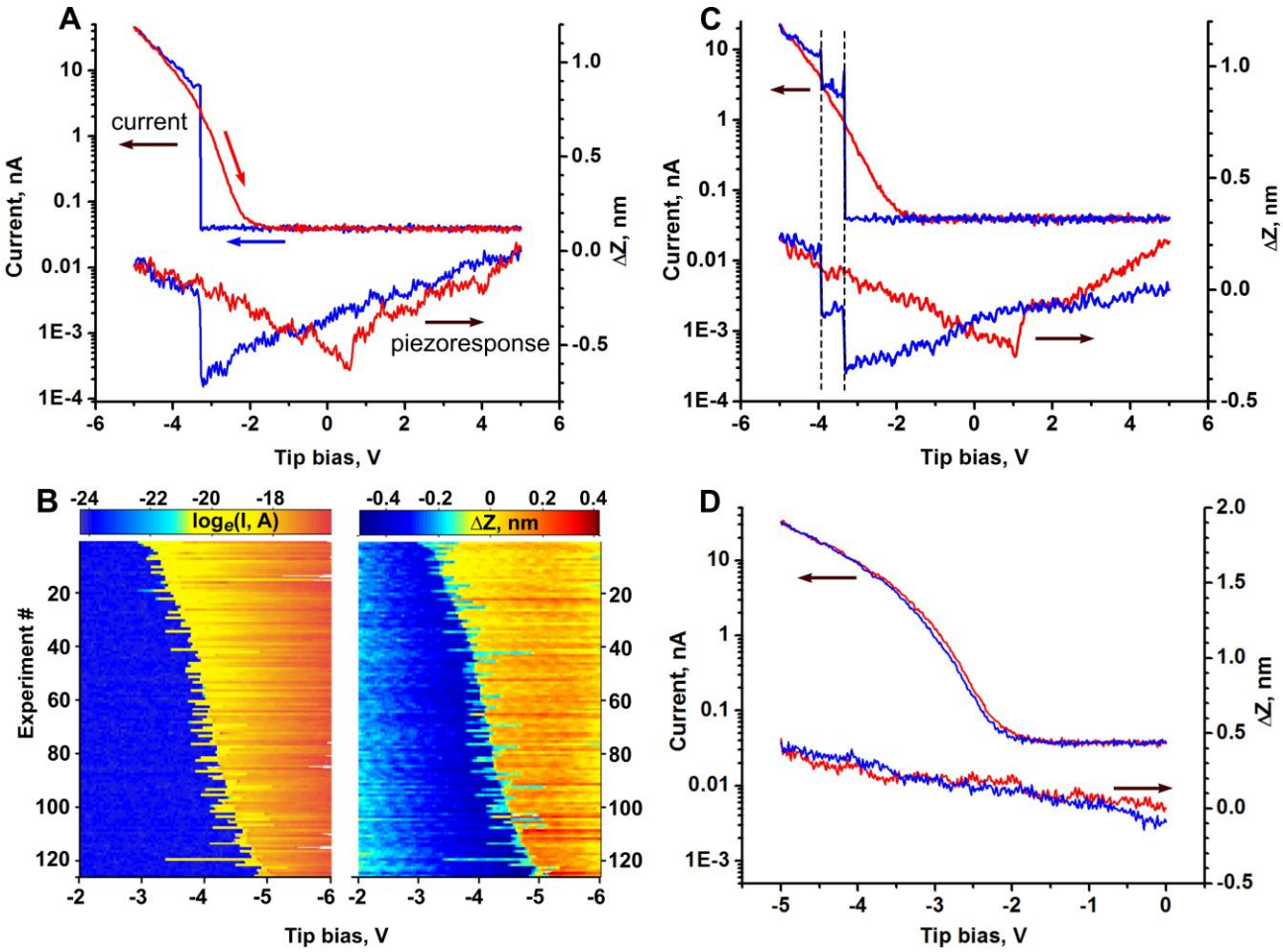
A
current
piezoresponse
Current, nA
ΔZ, nm
Tip bias, V
B
log_e(I, A)
ΔZ, nm
Experiment #
Tip bias, V
C
Current, nA
ΔZ, nm
Tip bias, V
D
Current, nA
ΔZ, nm
Tip bias, V

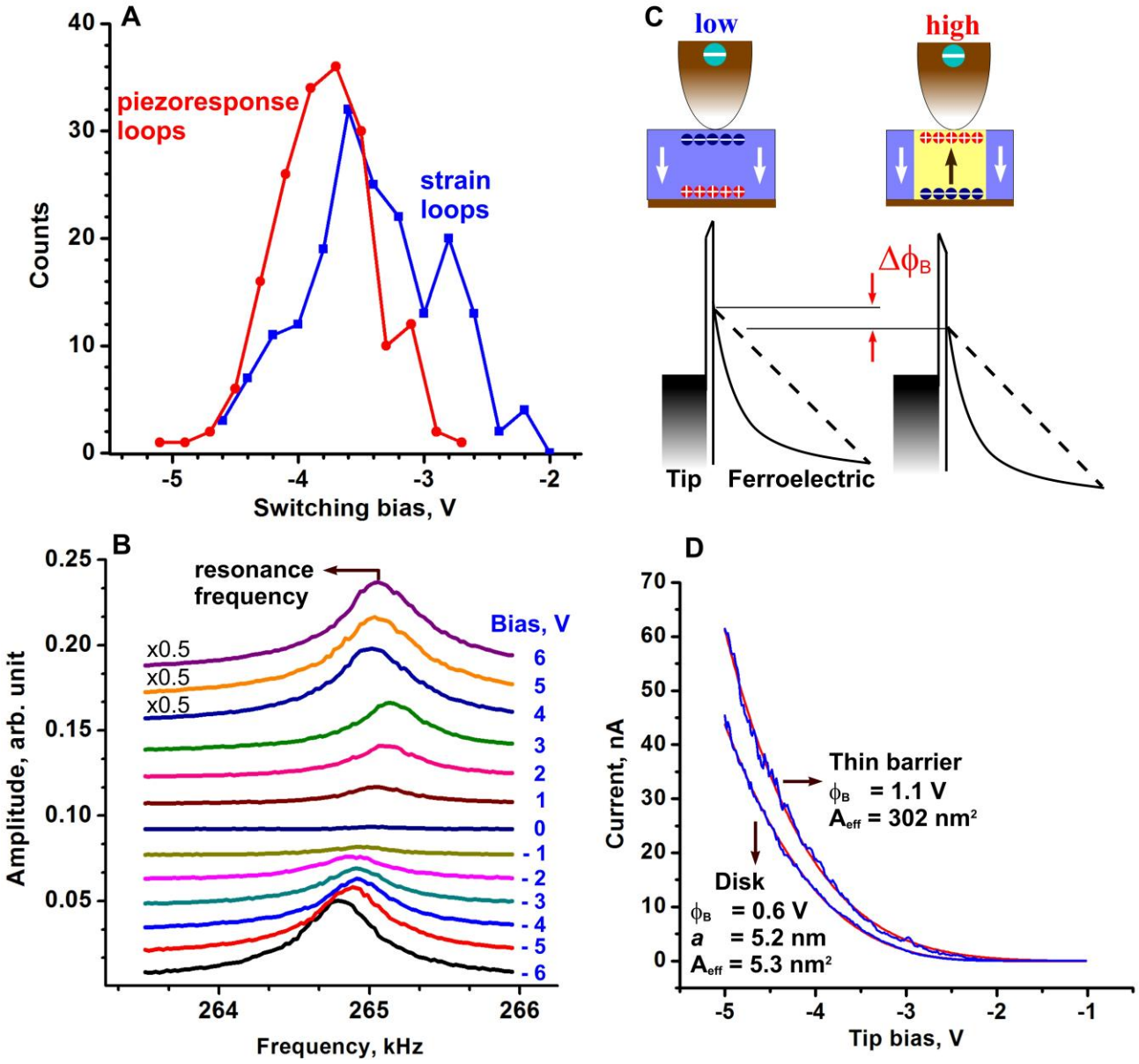
A
piezoresponse loops
strain loops
Counts
Switching bias, V
C
low
high
$\Delta\phi_B$
Tip
Ferroelectric
B
resonance frequency
Bias, V
x0.5
x0.5
x0.5
6
5
4
3
2
1
0
- 1
- 2
- 3
- 4
- 5
- 6
Amplitude, arb. unit
Frequency, kHz
D
Thin barrier
ϕ_B = 1.1 V
A_{eff} = 302 nm²
Disk
ϕ_B = 0.6 V
a = 5.2 nm
A_{eff} = 5.3 nm²
Current, nA
Tip bias, V

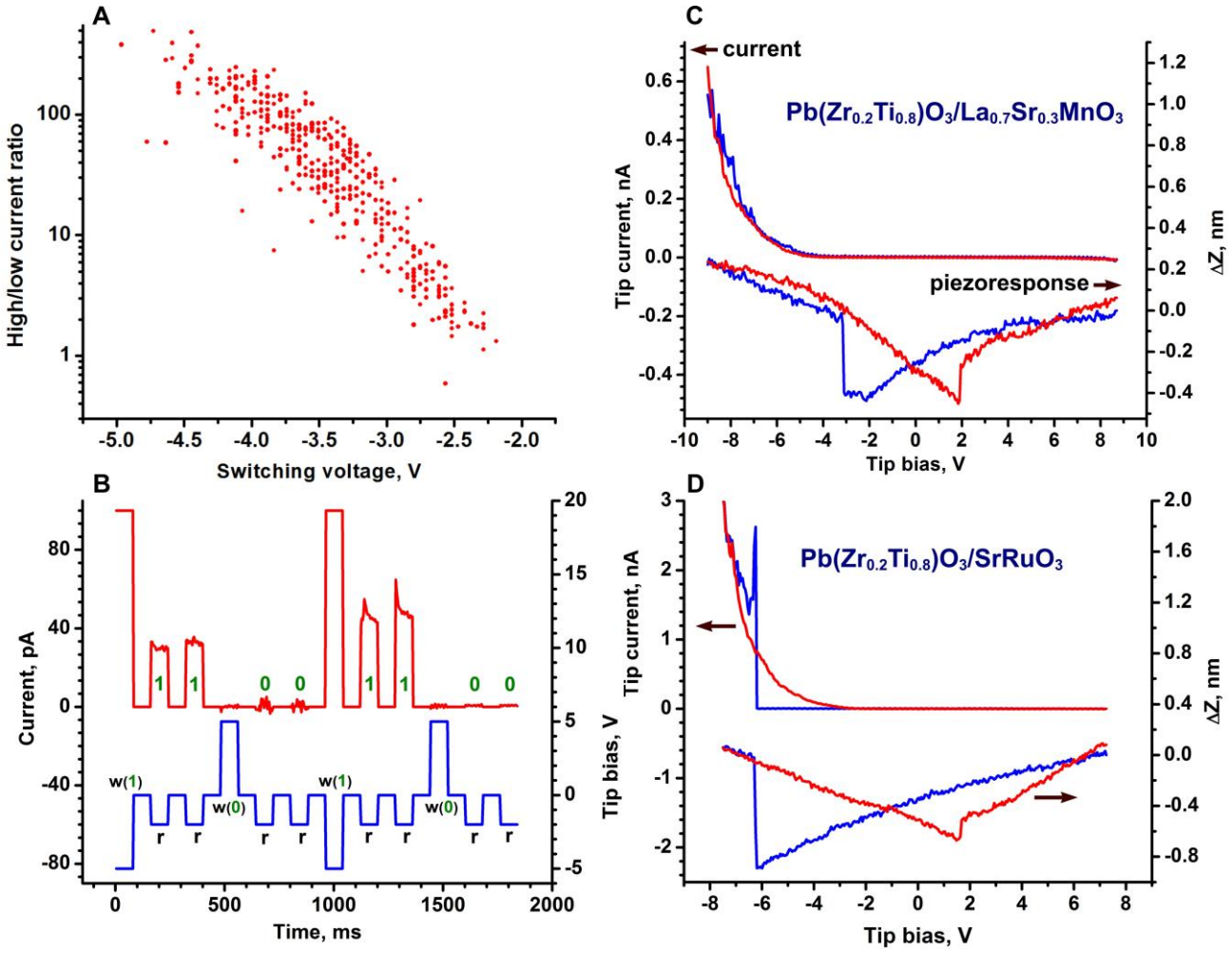
A
High/low current ratio
Switching voltage, V
B
Current, pA
Time, ms
w(1)
w(0)
r
C
current
piezoresponse
Pb(Zr0.2Ti0.8)O3/La0.7Sr0.3MnO3
Tip current, nA
ΔZ, nm
Tip bias, V
D
Pb(Zr0.2Ti0.8)O3/SrRuO3
Tip current, nA
Tip bias, V
ΔZ, nm